Two-Dimensional Electronic-Vibrational Spectroscopic Study of Conical Intersection Dynamics: An Experimental and Electronic Structure Study

Journal:	*Physical Chemistry Chemical Physics*
Manuscript ID	CP-ART-08-2018-005264.R1
Article Type:	Paper
Date Submitted by the Author:	27-Sep-2018

Complete List of Authors:	Wu, Eric; E O Lawrence Berkeley National Laboratory, Physical Biosciences Division; University of California Berkeley, Chemsitry Ge, Qinghui; University of California Berkeley, Chemsitry Arsenault, Eric; University of California Berkeley, Chemsitry; E O Lawrence Berkeley National Laboratory, Molecular Biophysics & Integrated Bioimaging Lewis, Nicholas; James Franck Institute Gruenke, Natalie; E O Lawrence Berkeley National Laboratory, Molecular Biophysics & Integrated Bioimaging; University of California Berkeley, Chemsitry Head-Gordon, Martin; University of California Berkeley, Chemsitry Fleming, Graham; E O Lawrence Berkeley National Laboratory, Molecular Biophysics & Integrated Bioimaging; University of California Berkeley, Chemsitry; Kavli Energy NanoScience Institute

Journal Name

ARTICLE

Two-Dimensional Electronic-Vibrational Spectroscopic Study of Conical Intersection Dynamics: An Experimental and Electronic Structure Study

Received 00th January 20xx,
Accepted 00th January 20xx

DOI: 10.1039/x0xx00000x

www.rsc.org/

Eric C. Wu[a,b], Qinghui Ge[a], Eric A. Arsenault[a,b], Nicholas H. C. Lewis[d], Natalie L. Gruenke[a,b], Martin J. Head-Gordon[a,]*, Graham R. Fleming[a,b,c,]†

The relaxation from the lowest singlet excited state of the triphenylmethane dyes, Crystal Violet and Malachite Green, is studied via two-dimensional electronic-vibrational (2DEV) spectroscopy. After excitation of the dyes at their respective absorption maxima, the ensuing excited state dynamics are tracked by monitoring the C=C aromatic stretch. With the aid of electronic structure calculations, the observed transitions in the 2DEV spectra are assigned to specific geometries and a detailed story of the evolution of the nuclear wavepacket as it diffuses on the excited state potential energy surface (PES) and ultimately passes through the conical intersection is developed. Notably, it is revealed that the relaxation of the lowest singlet excited state involves intramolecular charge transfer while the nuclear wavepacket is on the excited state PES. Finally, through analyzing the center line slopes of the measured peaks, we show how both solvent motions and changes in the molecular dipole moment affect the correlation between electronic and vibrational degrees of freedom. This work clearly demonstrates the usefulness of 2DEV spectroscopy in following the motion of nuclear wavepackets after photoexcitation and in studying the interactions between the molecular dipole moment and sourrounding solvent environment.

Introduction

Conical intersections[1–8] are points or seams of degeneracy between potential energy surfaces (PESs). Conical intersections play major roles in photochemical reactions and ultrafast radiationless decays, such as carotenoid $S_2 \rightarrow S_1$,[9–11] DNA bases,[12–15] cyanine dyes,[1,16] and rhodopsin isomerization.[17,18] Despite much study of conical intersections from simulation and theory, there are few experiments that can probe PESs near conical intersections.[16,17,19] Within the Born-Oppenheimer approximation, the nuclei move on adiabatic PESs. In the vicinity of conical intersections, strong nonadiabatic coupling between the states occurs, the Born-Oppenheimer approximation is no longer valid, and the motions of nuclei and electrons cannot be separated. The recently developed two-dimensional electronic-vibrational spectroscopy (2DEV) has potential for studies of conical intersection dynamics as it correlates the evolution of electronic and nuclear degrees of freedom.[20–25] 2DEV spectroscopy combines the advantages of 2D electronic spectroscopy and 2D infrared spectroscopy, as it enables the correlation of the initial electronic absorption with the subsequent evolution of the nuclear positions.

The relaxation from the lowest singlet excited state of triphenylmethane dyes, such as malachite green (MG) and crystal violet (CV) (Chart 1), is believed to involve a conical intersection and provide a tractable system to confront theory and experiments.[26,27] Past studies of these molecules have shown that excited state decay time of triphenylmethane dyes is viscosity dependent.[28,29] The radiationless relaxation of triphenylmethane dyes involves rotation of the phenyl rings, and a number of simulations and theoretical studies of MG and CV have been reported. Bagchi *et al.* modeled the relaxation of these dyes as motions on a one-dimensional potential surface without any barrier, with the decay of the excited state occurring at a sink in the potential surface.[30] Their model successfully described many aspects of the photophysics of these dyes, and the model attributed the fractional viscosity dependence of the nonradiative processes to the position of the sink.[30] Nakayama *et al.* performed simulations on MG with complete active space second order perturbation theory (CASPT2) and complete active space self-consistent field.[31] They found two different conical intersections between the S_0 and S_1 PESs. Furthermore, they found that there are two S_1 minima located near the two conical intersections, i.e. the structures at

[a] Department of Chemistry, University of California, Berkeley, California 94720, USA
[b] Physical Biosciences Division, Lawrence Berkeley National Laboratory, Berkeley, California 94720, USA
[c] Kavli Energy Nanosciences Institute at Berkeley, Berkeley, California 94720, USA
[d] James Franck Institute, University of Chicago, Illinois 60637, USA
* E-mail: mhg@cchem.berkeley.edu
† E-mail: grfleming@lbl.gov (Corresponding Author)
Electronic Supplementary Information (ESI) available: Details of calculated results and discussion on computational methods. See DOI: 10.1039/x0xx00000x

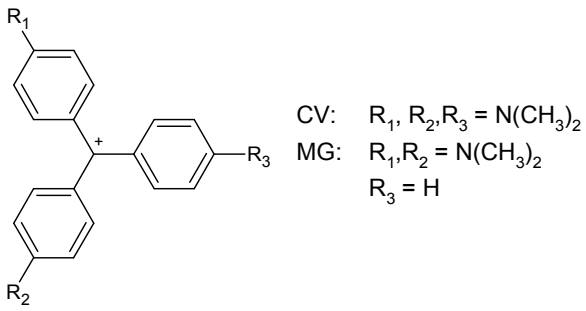

Chart 1. Structure of the triphenylmethane dyes, malachite green (MG) and crystal violet (CV).

the two S_1 minima are similar to the structures at the two conical intersections. Therefore, they concluded that once excited molecules relax to the S_1 minima from the Franck-Condon structure, small motions lead to the conical intersections and rapid return to ground state surface. Xie *et al.* performed simulations with multireference configuration interaction, a semi-empirical method.[32] They found an additional conical intersection, which is also located near an S_1 minimum. Using calculated gas phase trajectories, they reported an S_1 excited state lifetime of 1.2 ps, with no change in population during the first 300 fs, which they attributed to initial relaxation from the Franck-Condon region to the conical intersections. Experimentally, Li *et.al.* offered a different interpretation.[33] Using visible pump-infrared probe spectroscopy, they reported that the relaxation of MG involves intramolecular charge transfer. They concluded that following photoexcitation, the excited dye molecules relax from the locally excited state to the twisted intramolecular charge transfer state after ~4 – 5 ps, although this model can be considered as simply an alternative formulation of the models described above.

In this work, we performed two-dimensional electronic-vibrational spectroscopy on MG and CV in deuterated methanol and propanol. From the 2DEV spectra, we found evidences that the relaxation of CV and MG involves both intramolecular charge transfer (ICT) and conical intersection dynamics.

Experimental Methods

The 2DEV technique has been described in detail previously.[21] Briefly, the laser source was a Ti:Sapphire regenerative amplifier (Coherent; Legend Elite USP; 806 nm, 40 fs, 0.9 mJ, 1 kHz) seeded by a Ti:Sapphire oscillator (Coherent; Micra). The infrared (IR) beams were generated by a home-built optical parametric amplifier (OPA) via difference frequency generation and the visible beam was generated by a home-built non-collinear optical parametric amplifier (NOPA).

The OPA was tuned to generate IR pulses centered at 6.4 μm with a pulse duration ~100 fs. This beam was split by a 50:50 ZnSe beamsplitter to generate the probe and the reference beams, which were focused at the sample position by a $f = 15$ cm gold-coated 90° off-axis parabolic mirror. The reference beam was used to normalize the probe spectrum and to compensate for the instability in the laser intensity. The IR probe beam and the visible pump beam were overlapped at the sample using a 100-μm pinhole, and the reference beam was displaced to not overlap with the pump beam. After passing through the sample, the probe and reference beams were dispersed onto an imaging spectrometer (Horiba; Triax 180) and detected with a dual-array HgCdTe detector with 64 elements per array (Infrared Systems Development).

The NOPA was tuned to generate broadband pulses spanning ~480 – 850 nm. The beam passed through an acousto-optic programmable dispersive filter (AOPDF) (Fastlite; Dazzler) to shape and compress the pulses. For the CV samples, the pump beam was tuned to ~300 μW and 75 nm bandwidth centered at 580 nm, and, for the MG samples, the pump beam was tuned to ~300 μW at 75 nm bandwidth centered at 600 nm. For both samples, the pulses were compressed to ~30 fs. The AOPDF was additionally used to split the visible pump into two degenerate pulses, with a controllable time delay t_1 and phase ϕ_1 between the two pulses. After passing through the AOPDF, the pump beam was reflected off a retroreflector on a controllable delay stage to control the waiting time t_2 between the pump and the probe pulses. The pump beam was focused at the sample position with a $f = 25$ cm silver coated 90° off-axis parabolic mirror.

For a given waiting time between the pump and the probe pulses, a 2DEV spectrum was acquired by scanning t_1, the delay time between the two degenerative pump pulses, from 0 – 100 fs in 2.4 fs steps and the desired signal was isolated by phase cycling with respect to ϕ_1 in a $3 \times 1 \times 1$ phase cycling scheme. The pump frequency was acquired by performing a Fourier Transform over t_1. The signal was collected in the fully rotated frame with respect to t_1 to remove the optical frequency of the pump laser.[34,35]

Results

First, we describe the 2DEV spectra of CV and MG in deuterated methanol. For CV (Figure 1), three peaks were observed at $t = 250$ fs, with a fourth peak appearing after $t = 2.5$ ps. All four peaks have their maxima on the visible axis at 1.70×10^4 cm^{-1}, which is near the λ_{max} of CV. The positive peak (red contours) initially at 1595 cm^{-1} is assigned to the ground state bleach of an aromatic C=C stretch. The assignment of the negative peaks (blue contours) at 1513 cm^{-1}, ~1575 cm^{-1}, and ~1587 cm^{-1} will be discussed below. As the peak initially at 1586 cm^{-1} grew, it blueshifted from 1586 cm^{-1} at $t = 2.5$ ps to 1589 cm^{-1} at $t = 15$ ps. The ground state peak also blueshifted from 1595 cm^{-1} at $t = 250$ fs to 1598 cm^{-1} at $t = 15$ ps. The blueshift of the ground state peak is due to the overlap of the ground state bleach and the peak at ~1587 cm^{-1}, where the blueshift of the latter causes the ground state peak to also blueshift. The peak initially at 1573 cm^{-1} was initially broad, then sharpened and slightly blueshifted from 1573 cm^{-1} to 1577 cm^{-1}. The peak at 1513 cm^{-1} did not blueshift or sharpen.

For MG in deuterated methanol (Figure 2), four peaks were observed in the 2DEV spectrum at $t = 500$ fs. These peaks are located at 1.67×10^4 cm^{-1} on the visible axis and at 1513 cm^{-1}, 1574 cm^{-1}, 1595 cm^{-1}, and 1618 cm^{-1} on the IR axis. An additional peak appeared at $t = 1$ ps at 1.67×10^4 cm^{-1} on the visible axis and 1585 cm^{-1} on the IR axis. As in the 2DEV spectrum of CV, the positive (red) bleach at 1595 cm^{-1} is assigned to an aromatic C=C stretch in the ground state. The assignments of the four negative (blue) peaks are discussed below. With increasing waiting time, the ground state band initially at 1595 cm^{-1} blueshifted to 1598 cm^{-1} and the absorption initially at 1585 cm^{-1} blueshifted to 1589 cm^{-1}. As previously discussed for CV, the observed blueshift of the ground state peak is due to the overlap of the ground state bleach and the absorptive signal at 1585 cm^{-1}. The peak initially at 1574 cm^{-1} was initially broad, then sharpened and blueshifted to 1577 cm^{-1}. In the discussion below, peaks will be identified using the frequencies at the

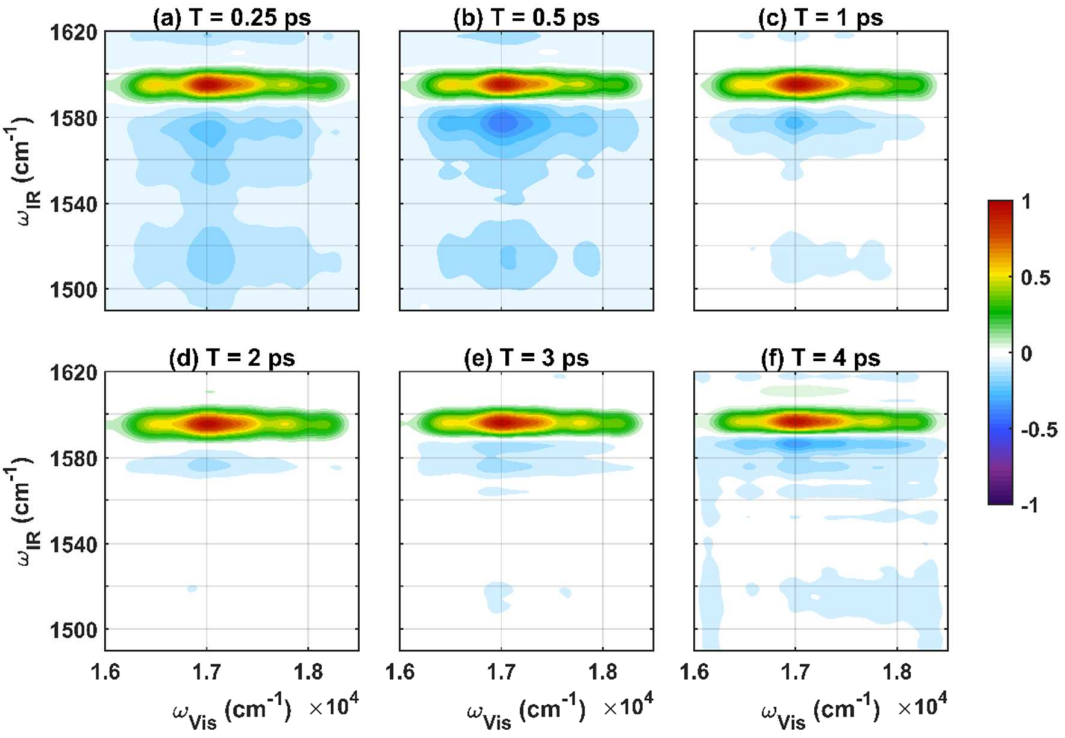

Figure 1. 2DEV spectra of CV in deuterated methanol at (a) 250 fs, (b) 500 fs, (c) 1 ps, (d) 2ps, (e) 3 ps, and (f) 4 ps. Red contours correspond to a bleach/stimulated emission; red contours to induced absorption. Each waiting time has been normalized such that the maximum intensity for each waiting time is one.

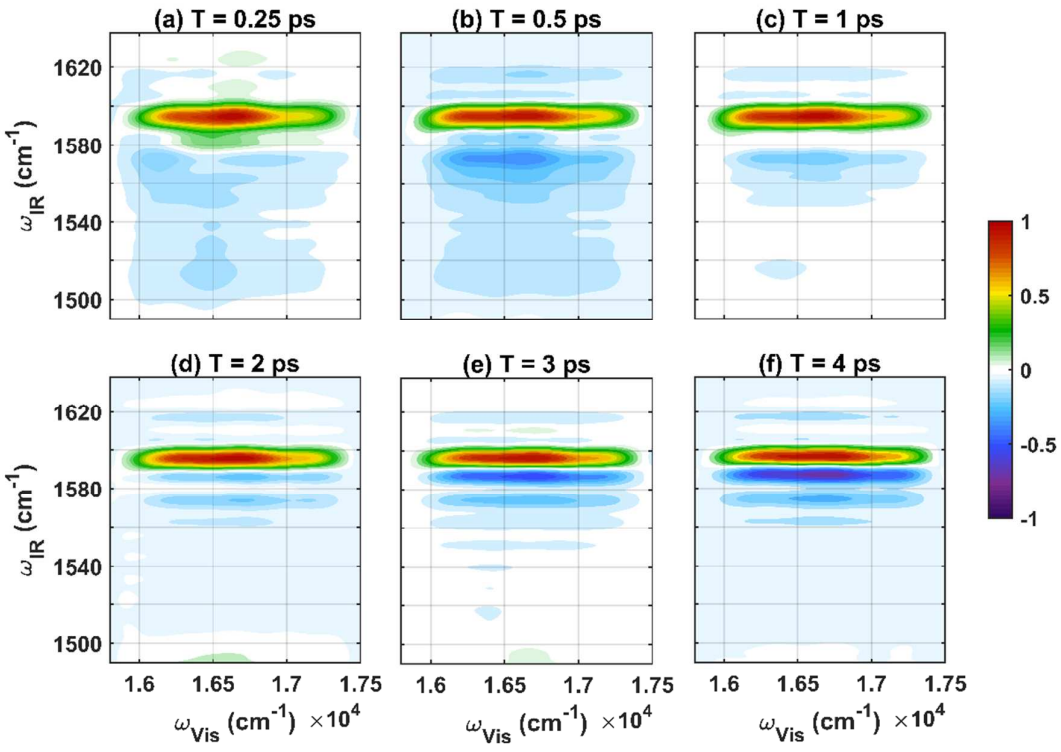

Figure 2. 2DEV spectra of MG in deuterated methanol at (a) 250 fs, (b) 500 fs, (c) 1 ps, (d) 2 ps, (e) 3 ps, and (f) 4 ps. Each waiting time has been normalized such that the maximum intensity for each waiting time is one.

longest waiting time measured.

We performed *ab initio* calculations to locate the minimum energy structures on the ground and excited potential energy surfaces of CV and MG, and obtained the vibrational frequencies within the harmonic oscillator approximation. Spin-flip time-dependent density functional theory (SF-TDDFT)[36] with the Tamm-Dancoff approximation[37] were employed for ground and excited state energy and property calculations. Alternatively, we have utilized TDDFT[38–41] and ΔSCF-DFT[42] to compute excited states, which take regular DFT ground states as references. A comparison of these methods and a discussion on how solvents would affect the calculated results can be found in the supporting information. All calculations use the BHHLYP[43] (which is recommended for SF-TDDFT calculations)[36] or B3LYP functionals and Pople's 6-31G(d) basis set,[44] and were performed with the Q-Chem 5.0 quantum chemistry package.[45]

With SF-BHHLYP, the optimized geometry for ground state CV and MG ($S_{0,eq}$) has a D3 (or D3-like) symmetry. For the S_1 excited state, the geometry minima have two rings perpendicular to the other. There are two such minima for MG, which we referred to as $S_{1,min}$ and $S_{1,min}$', respectively, and only one such minimum ($S_{1,min}$) for CV due to the equivalence of the three rings. It should be noted that TDDFT and ΔSCF-DFT find an additional minimum (denoted as $S_{1,meta}$) that has one ring perpendicular to the plane formed by the central carbon and carbons connected to it. We also located the minimal energy crossing points (MECP) for CV and MG using SF-TDDFT, the structures of which have similar characters to S_1 or $S_{1,min}$'. All energies and frequencies of these structures are summarized in Table 1.

Based on the calculated geometries and energies, Figure 4 shows a schematic of the PESs for the two triphenylmethane dyes. One notable difference between CV and MG is that for CV the Franck Condon structure ($S_{1,FC}$) has a higher energy than $S_{1,min}$, while for MG, the order is reversed. This may indicate the existence of a transition state between $S_{1,FC}$ and $S_{1,min}$. With TDDFT and ΔSCF-DFT, the energy of $S_{1,meta}$ is very close to that of the $S_{1,FC}$ (see the ΔSCF-DFT result in SI), suggesting that the PES around the Franck-Condon region is quite flat and whether or not $S_{1,meta}$ exists is sensitive to different computational

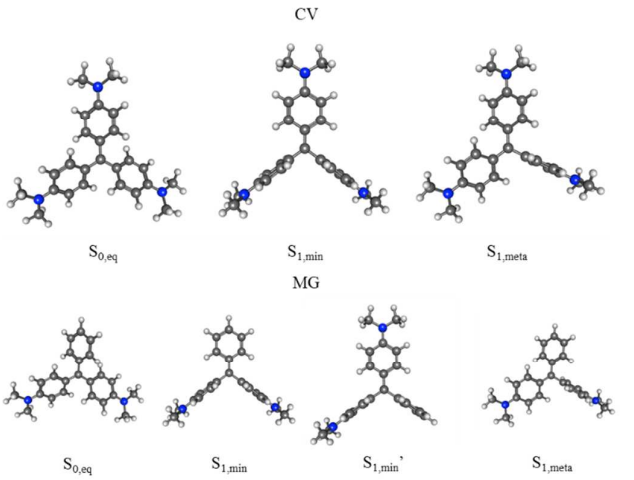

Figure 3. Optimized geometries for CV and MG.

Table 1. Energies and frequencies of the C=C aromatic stretch for CV and MG at the various optimized geometries computed with SF-BHHLYP and 6-31G(d) basis. The energies are referenced to the ground state energy of S_0. The numbers in parentheses are CASPT2 energies taken from Ref. 31.

Structure	$E(S_0)$ (eV)	$E(S_1)$ (eV)	Freq. (cm^{-1})	Int. (km/mol)
CV				
$S_{0,eq}$	0	2.33	1724	2716
$S_{1,min}$	1.37	2.28	1694	6228
MECP	2.71		-	-
MG				
$S_{0,eq}$	0	1.91(2.02)	1713	1209
$S_{1,min}$	2.00	2.10(2.14)	1679	6122
$S_{1,min}$'	1.11	2.42(2.37)	1713, 1726	237, 629
MECP	2.11(2.39)		-	-

methods. After the initial photoexcitation, the excited molecule first relaxes to the $S_{1,meta}$ geometry, then to the $S_{1,min}$ geometry. Once the molecule reaches the $S_{1,min}$ geometry, it goes through a conical intersection located near the $S_{1,min}$ and relaxes to the twisted ground state ($S_{0,twist}$). Finally, the molecule returns from the $S_{0,twist}$ to the $S_{0,eq}$ geometry through twisting of the aniline rings.

To identify the absorptive (blue) peaks, we examine 2DEV peak intensities as a function of time for both systems in two different solvents (Figure 5). The fitted decay times are listed in Table 2. For both CV and MG in methanol, all peaks, except for the peak at 1589 cm^{-1} for both and the peak at 1577 cm^{-1} for CV, decayed monotonically toward zero. The intensity of the peak at 1589 cm^{-1} increased during the first few picoseconds after the peak appears, then decays toward zero. For the 1577-cm^{-1} peak of CV, from 250 to 500 fs, the peak intensity (arbitrary units throughout) increased from 0.008 ± 0.001 to 0.015 ± 0.001, then decayed exponentially toward zero. To extract the decay times, the peak heights were fitted with one- or two- component exponential functions. However, it is important to note that peak height is representative of both population and vibrational oscillator

strength. As the nuclear wavepacket evolves on the excited state PES, the *ab initio* calculation (Table 1) shows that vibrational oscillator strength increases during relaxation from the Franck-Condon ($S_{1,FC}$) geometry to $S_{1,min}$ geometry.

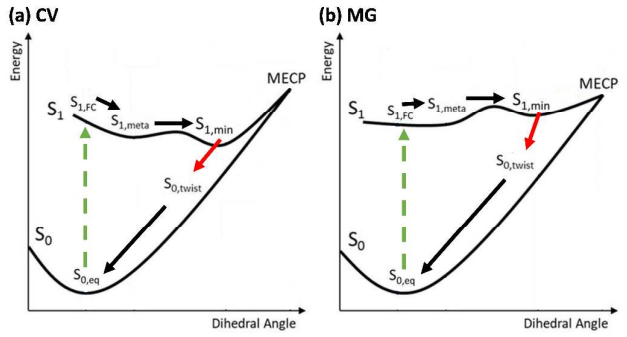

Figure 4. Schematic potential energy surfaces for (a) CV and (b) MG. The surfaces and the barriers are not drawn to scale. $S_{1,FC}$ and $S_{0,eq}$ refer to the same geometry, but on different PESs. Same for $S_{1,min}$ and $S_{0,twist}$.

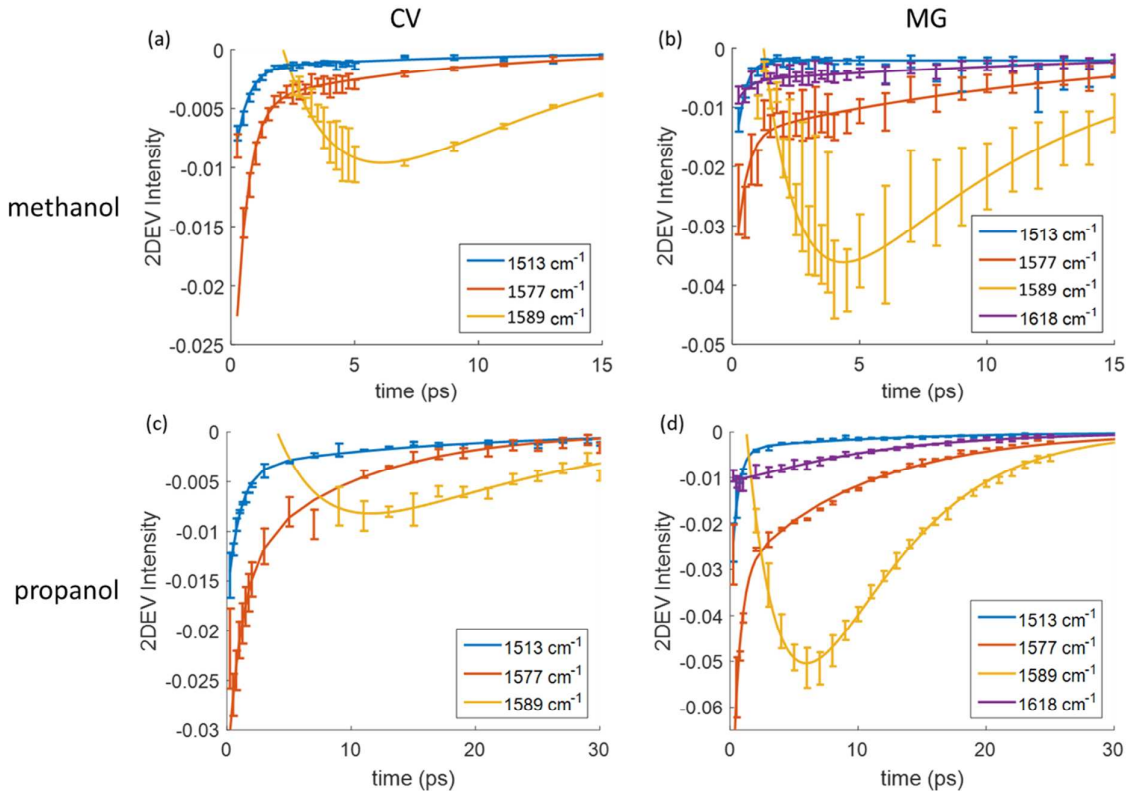

Figure 5. 2DEV peak intensities as a function of time for (a) CV and (b) MG in methanol, and for (c) CV and (d) MG in propanol. The solid line is the fitted result with a two-exponential function.

Table 2. Decay times for 2DEV intensities and k_{vis}'s of CV and MG in methanol and propanol. All times are in ps. For those peaks whose intensities are better fitted with two-exponential functions, the amplitude of the short component is listed in parentheses. The decays of k_{vis} can be fitted with a single-exponential function.

	CV		MG	
	Methanol	Propanol	Methanol	Propanol
2DEV Intensity				
1513 cm^{-1}	$0.51(0.87) \pm 0.6$ 12 ± 1	$1.0(0.78) \pm 0.1$ 17 ± 3	0.32 ± 0.06	$0.52(0.90) \pm 0.03$ 12 ± 1
1577 cm^{-1}	$0.50(0.87) \pm 0.04$ 8.0 ± 0.3	$1.1(0.60) \pm 0.2$ 9.8 ± 1.0	$0.39(0.67) \pm 0.17$ 13 ± 2	$0.55(0.68) \pm 0.07$ 9.9 ± 0.4
1589 cm^{-1}	2.8 ± 0.9 (rise) 6.0 ± 1.3	4.5 ± 3.1 (rise) 14 ± 6	1.5 ± 0.2 (rise) 7.9 ± 0.8	3.7 ± 0.5 (rise) 6.0 ± 0.7
1598 cm^{-1}	5.2 ± 0.2	8.9 ± 1.8	8.1 ± 0.4	7.1 ± 0.3
1618 cm^{-1}	-	-	$0.43(0.50) \pm 0.23$ 17 ± 3	10 ± 1
k_{vis}				
1577 cm^{-1}	-	-	0.96 ± 0.29	2.5 ± 0.4
1589 cm^{-1}	1.3 ± 0.5	-	0.70 ± 0.13	3.7 ± 2.5
1598 cm^{-1}	2.2 ± 0.4	7.9 ± 1.6	1.6 ± 0.4	2.9 ± 0.7

For CV in methanol (Figure 5a), the decay of the ground state peak (not shown) can be reasonably fitted ($R^2 = 0.98$) with a single exponential function, $A\exp(-t/\tau)$, with $\tau = 5.2 \pm 0.2$ ps. The two negative peaks at 1513 cm^{-1} and 1577 cm^{-1} are better fitted with a biexponential function, $A_1\exp(-t/\tau_1) + A_2\exp(-t/\tau_2)$, with R^2 of 0.98 and 0.99, respectively. For the

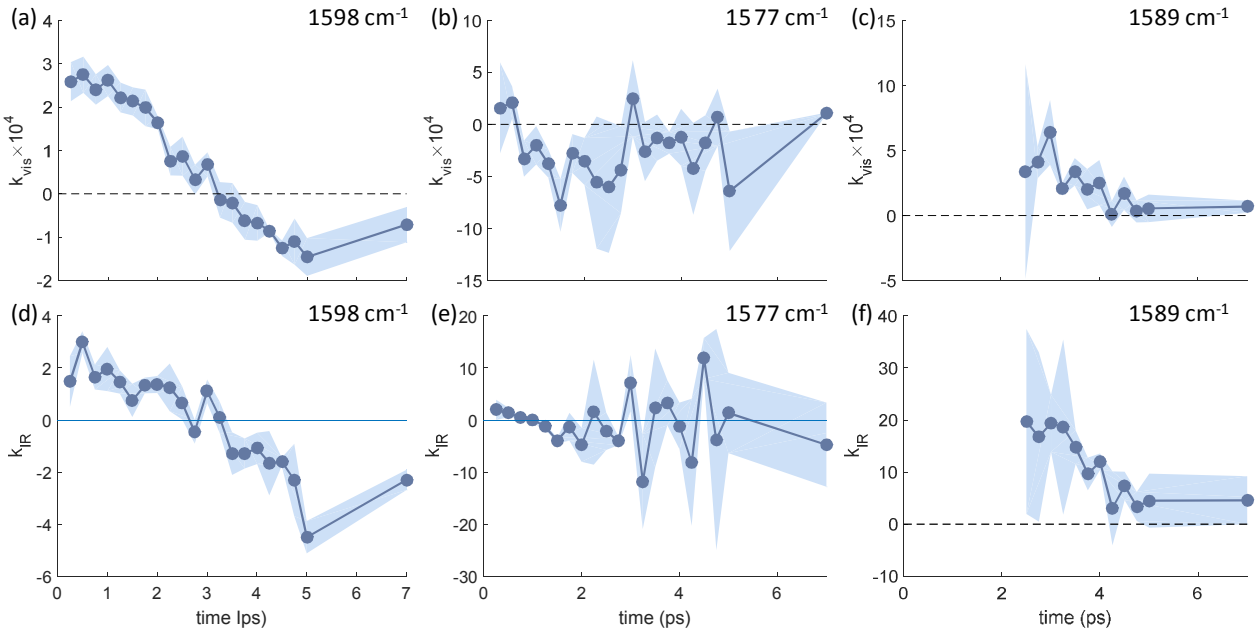

Figure 6. Center line slopes as a function of time for CV in methanol. The top row shows k_{vis} for the peaks at (a)1598 cm^{-1} ($S_{0,eq}$), (b)1577 cm^{-1} ($S_{1,min}$), and (c)1589 cm^{-1} ($S_{0,twist}$). The bottom row shows k_{IR} for (d)1598 cm^{-1} ($S_{0,eq}$), (e)1577 cm^{-1} ($S_{1,min}$), and (f)1589 cm^{-1} ($S_{0,twist}$). The shaded area represents the standard error.

peak at 1513 cm^{-1}, the amplitude-weighted average lifetime was fit to be 2.0 ± 0.2 ps. On the other hand, for the peak at 1577 cm^{-1}, the amplitude-weighted average lifetime was found to be 1.5 ± 0.1 ps. The fast component of the 1513-cm^{-1} and 1577-cm^{-1} peaks are identical within experimental error, but the 1513-cm^{-1} peak has a longer slow component. For the fitting of the 1577 cm^{-1} peak, the point at $t = 250$ fs was ignored, because the intensity increased from at 250 fs to at 500 fs. The peak at 1589 cm^{-1} can be fitted with one rise component and one decay component, $A_{rise}\exp(t/\tau_{rise}) + A_{decay}\exp(-t/\tau_{decay})$, with $\tau_{rise} = 2.8 \pm 0.9$ ps and $\tau_{decay} = 6.0 \pm 1.3$ ps. Based on the potential surface, if this peak represents a geometry close to $S_{1,min}$ on either the S_1 or S_0 surfaces, we would expect, in addition to a rise, a delay in the appearance of this feature. Using the zero-point crossing as the starting point and the fitted function, we estimate the 1589-cm^{-1} peak first appears at ~2.1 ps.

For MG in methanol (Figure 5b), the ground state peak (not shown) has a decay time of 8.1 ± 0.4 ps. The peak at 1513 cm^{-1} can be fitted with a single exponential function with $\tau = 0.32 \pm 0.06$ ps. For the peaks at 1577 cm^{-1} and at 1618 cm^{-1}, the amplitude weighted averaged lifetimes are 4.7 ± 1.7 ps and 9.0 ± 3.5 ps, respectively. The long average lifetimes for those two peaks are due to slowly decaying components. The fast components for those two peaks are 0.39 ± 0.17 ps and 0.43 ± 0.23 ps, respectively. For the peak at 1589 cm^{-1}, the rise and decay times are 1.5 ± 0.2 ps and 7.9 ± 0.8 ps, respectively. Using the zero-point crossing and the fitted function, this peak is estimated to appear at ~1.2 ps.

The viscosity of propanol is four times that of methanol. For CV, the average lifetimes of all the peaks and the rise time of the 1589-cm^{-1} peak increased by factors ranging from 1.5 to 3, when methanol was replaced with propanol. In addition to the increase in the lifetimes of the peaks, the appearance of the 1589-cm^{-1} band was delayed from 2.1 ps in methanol to 4.1 ps in propanol. Since the relaxation occurs through the twisting of the phenyl rings, we would expect a more viscous solvent to decrease the decay rates of peak intensities.[31,32].

For MG, the average lifetimes for the peaks at 1513 cm^{-1} and 1618 cm^{-1} increased when methanol was replaced with propanol. However, the average lifetimes for the 1598-cm^{-1} and 1577-cm^{-1} peaks and the decay of the 1589-cm^{-1} peak decreased. For the 1577-cm^{-1} peak, the lifetime of the fast component increased, but the lifetime of the long component decreased in propanol versus methanol. Moreover, while the 1577-cm^{-1} and 1618-cm^{-1} peaks decayed monotonically in methanol, the intensities of those two peaks initially increased in propanol. For the 1577-cm^{-1} peak, the intensity increased from 0.027 ± 0.007 at 250 fs to 0.056 ± 0.008 at 500 fs. For the 1618-cm^{-1} peak, the intensity increased from 0.010 ± 0.001 at 250 fs to 0.012 ± 0.001 at 500 fs. In addition, the appearance of the 1589-cm^{-1} peak was delayed slightly from 1.2 ps in methanol to 1.3 ps in propanol, but the increase in the delayed appearance of this peak between the two solvents was not as pronounced for MG as that for CV.

Since the decay of peak intensity is a convolution of the change in vibrational oscillator strength and the decay in population, we cannot assign the peaks based solely on lifetimes. For example, even though the average lifetime of the 1618-cm^{-1} peak is twice of that of the 1577-cm^{-1} peak for MG in methanol, we cannot assume that those two peaks are from different geometries. However, using the dynamics of the intensity curves, we can tentatively assign the peaks to the optimized excited state geometries for both CV and MG. First, because the 1513-cm^{-1} peak decayed monotonically in all four molecule/solvent systems, while the 1577-cm^{-1} peak intensity

increased from 250 fs to 500 fs in three of the four systems, the 1513 cm^{-1}-peak is likely the $S_{1,meta}$ geometry, which is the excited state geometry closest to the Franck-Condon geometry ($S_{1,FC}$), and the peak at 1577 cm^{-1} (and 1618 cm^{-1} for MG) likely corresponds to the $S_{1,min}$ geometry, the geometry with the lowest energy on the excited state PES. Next, for MG, both the 1577-cm^{-1} and 1618-cm^{-1} peaks increased from 250 fs to 500 fs, then decayed after 500 fs, which could suggest that the two peaks arise from the same geometry. The difference in decay times of those two peaks could arise from differences in the evolution of the oscillator strengths. The 1577 cm^{-1} and 1618 cm^{-1} peaks did not increase in amplitude initially for MG in methanol, probably because the rise time of those peaks is shorter than 250 fs. Finally, the 1589-cm^{-1} peak is likely the twisted ground state geometry ($S_{0,twist}$). The increased delay in the appearance of the 1589-cm^{-1} peak is consistent with the idea that more time is needed for the wavepacket to reach the conical intersection.

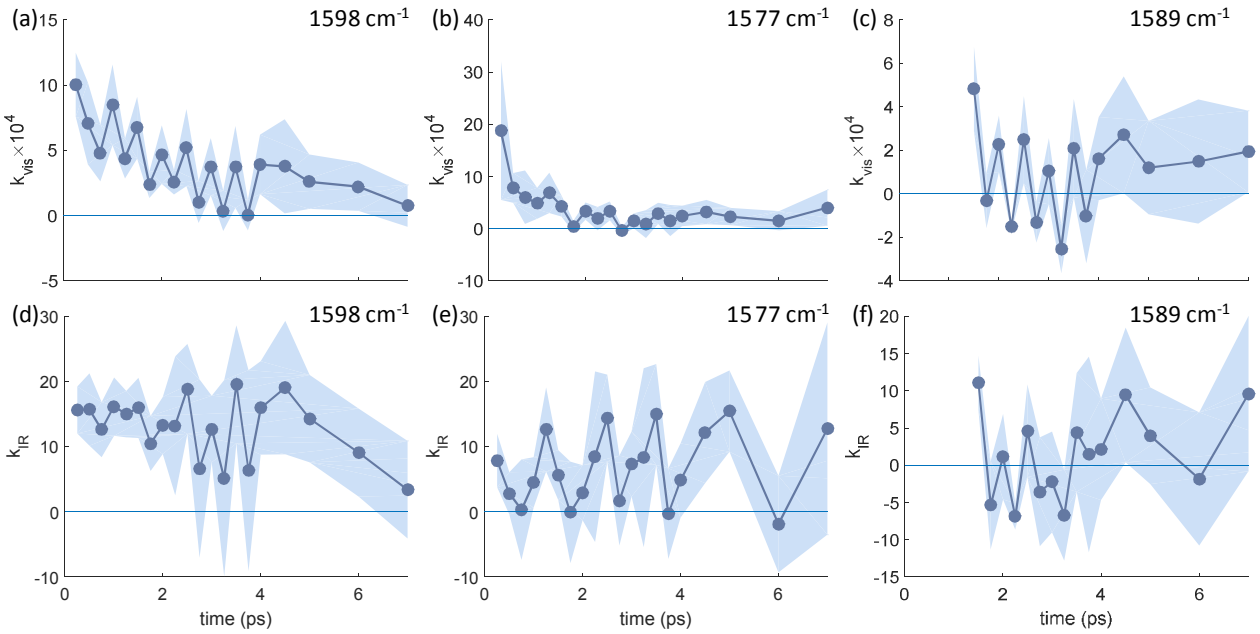

Figure 7. Center line slopes as a function of time for MG in methanol. The top row shows k_{vis} for the peaks at (a)1598 cm^{-1} ($S_{0,eq}$), (b)1577 cm^{-1} ($S_{1,min}$), and (c)1589 cm^{-1} ($S_{0,twist}$). The bottom row shows k_{IR} for (d)1598 cm^{-1} ($S_{0,eq}$), (e)1577 cm^{-1} ($S_{1,min}$), and (f)1589 cm^{-1} ($S_{0,twist}$). The shaded area represents standard error.

Discussion

Center Line Slopes

Here, we examine the dynamics of center line slopes (CLSs) – the slope of the spectral feature with respect to either of the two frequency axes. There are two different ways to define the CLS. Throughout, k_{vis} will be used to denote that the slope is calculated with respect to the visible frequencies, and k_{IR} will be used to denote that the slope is calculated with respect to the IR frequencies. CLSs contain various types of information. First, the center line slope indicates whether the electronic and vibrational transition energies are positively, negatively, or uncorrelated. Second, the decay of the center line slope gives a direct measurement of the vibrational dephasing time. Lastly, the magnitude of the center line slope can be used to estimate the relative strength with which a vibration couples to the bath on an electronically excited state versus ground state.[20,22] According to the analysis of Lewis *et al.*,[20]

$$\alpha_0 = k_{\mathrm{IR,\,GS}}(0) \tag{1}$$

$$\alpha_1 = \frac{k_{\mathrm{IR,\,GS}}(0)}{k_{\mathrm{IR,\,ES}}(0)} + k_{\mathrm{IR,\,GS}}(0) \tag{2}$$

where $k_{\mathrm{IR,\,GS}}$ and $k_{\mathrm{IR,\,ES}}$ are the k_{IR} for the ground and excited state, respectively, and α_0 and α_1 denote how the vibrational bath coupling is rescaled for the 0th and 1st vibrational levels on the electronic excited state as compared to the ground state.

CLSs were previously calculated by linear fitting of the maxima along either the visible axis or the IR axis.[9,20,22] However, for situations where the peaks are asymmetric, conditional averages give much more reliable CLSs. The conditional averages, $f(\omega_{\mathrm{vis}})$ and $g(\omega_{\mathrm{IR}})$, are calculated as follows:

$$f(\omega_{\mathrm{vis}}) = \frac{\int d\omega_{\mathrm{IR}} P(\omega_{\mathrm{vis}}, \omega_{\mathrm{IR}})\omega_{\mathrm{IR}}}{\int d\omega_{\mathrm{IR}} P(\omega_{\mathrm{vis}}, \omega_{\mathrm{IR}})} \tag{3}$$

$$g(\omega_{\mathrm{IR}}) = \frac{\int d\omega_{\mathrm{vis}} P(\omega_{\mathrm{vis}}, \omega_{\mathrm{IR}})\omega_{\mathrm{vis}}}{\int d\omega_{\mathrm{vis}} P(\omega_{\mathrm{vis}}, \omega_{\mathrm{IR}})} \tag{4}$$

where $P(\omega_{\mathrm{vis}}, \omega_{\mathrm{IR}})$ is the 2DEV intensity at $(\omega_{\mathrm{vis}}, \omega_{\mathrm{IR}})$. $f(\omega_{\mathrm{vis}})$ and $g(\omega_{\mathrm{IR}})$ are calculated for the range of frequencies that encloses the peak. Then, k_{vis} or k_{IR} can be calculated by fitting $f(\omega_{\mathrm{vis}})$ or $g(\omega_{\mathrm{IR}})$ versus ω_{vis} or ω_{IR} to linear functions. For asymmetric peaks, when the CLSs are calculated using the maxima, k_{vis} and k_{IR} do not have the same decay rate. This suggests that there are two different vibrational dephasing times for the same vibrational mode, which is physically impossible. When CLSs are calculated using the conditional averages, k_{vis} and k_{IR} have a similar decay rate, as Lewis *et al.* observed for DTTCI.[20]

By using the conditional averages to calculate the CLSs, k_{vis} and k_{IR} of CV in methanol had similar decay rates (we discuss the sign of the of the CLSs below). The decay times of k_{vis} for CV and MG are listed in Table 2. The decay times are 2.2 ± 0.4 ps and 2.1 ± 0.5 for the ground state k_{vis} and k_{IR}, respectively, and 1.3 ± 0.5 ps and 1.6 ± 0.3 ps for the $S_{0,\mathrm{twist}}$ k_{vis} and k_{IR}, respectively. Interestingly, the CLS for the C=C stretch has a slightly different decay time for the ground state and for the twisted ground state. The CLSs of the excited state are significantly different from those of the other two ground state modes. The decay of both k_{IR} and k_{vis} is not exponential, rather both appear to become more negative from 0 to 2 ps, then decay toward zero after 2 ps. A rise is not observed for either k_{vis} or k_{IR} for the other two peaks, but they do appear to plateau as waiting time approaches zero.

Since the excited state CLS has large uncertainties, we only use the ground state k_{IR} to estimate $\alpha_0 = 1.5 \pm 0.9$ for CV, i.e. the reorganization energy of the 0th vibrational level is rescaled by a factor of $\alpha_0^2 = 2.3$ on the electronic excited state.[20]

Figure 7 shows the dynamics of k_{vis} for MG. The decays of k_{vis} for $S_{0,\mathrm{eq}}$, $S_{0,\mathrm{twist}}$, and $S_{1,\mathrm{min}}$ can be fitted with a single exponential function. The decay times are 1.6 ± 0.4 ps, 0.70 ± 0.13 ps, and 0.96 ± 0.29 ps for $S_{0,\mathrm{eq}}$, $S_{1,\mathrm{min}}$, and $S_{0,\mathrm{twist}}$, respectively. Due to the large uncertainties, k_{IR} cannot be fitted with an exponential decay function. Unlike the CLSs for CV, the k_{vis}'s for MG do not appear to plateau as waiting time approaches zero.

The ground state and excited state k_{IR}'s give $\alpha_0 = 16 \pm 4$ and $\alpha_1 = 18 \pm 4$, which means that the reorganization energies of the 0th and 1st vibrational levels are rescaled by a factor of 260 and 320 on the electronic excited state, respectively. Those rescaling factors seem unphysical, but there are large uncertainties in the values of k_{IR} at a waiting time of zero, $k_{IR}(0)$.

For both CV and MG, the uncertainties in the values of k_{IR} are larger than those for k_{vis}. The larger uncertainties in the values of k_{IR} are due to the narrow width of the peak along the IR axis. Typically, k_{IR} is calculated by fitting ~30 data points, whereas k_{vis} is calculated by fitting ~200 data points. Therefore, the calculation of k_{IR} is significantly more affected by the noise in the 2DEV spectrum than the calculation of k_{vis}.

We consider the solvent dependence of the CLSs using the ground state k_{vis} of CV as the example. The decay time of k_{vis} increased from 2.2 ± 0.4 ps to 7.9 ± 1.6 ps when the solvent was changed from methanol to propanol. This decay time increase is very similar to the increase in the viscosity of the solvent. In a more viscous solvent, the memory of the correlation lasts longer, therefore, the decay time of the CLS becomes longer. The values of $k_{\mathrm{vis}}(0)$, k_{vis} at waiting time of zero, are the same in methanol and in propanol. This suggests that vibration-bath couplings are scaled by the same factor in both solvents.

One of the most noticeable differences between CV and MG is the sign of the CLS. For MG, all three CLSs are positive and decay monotonically toward zero. On the other hand, for CV, the CLSs of $S_{0,\mathrm{eq}}$ and $S_{0,\mathrm{twist}}$ are positive and decay monotonically toward zero, but the CLS of $S_{1,\mathrm{min}}$ starts at zero, becomes negative, then decays back toward zero. The difference in the signs of the CLSs can be understood by considering the molecular dipole moment.

For CV, $S_{0,\mathrm{eq}}$ has no dipole moment with respect to the center of charge, because it is symmetric. Therefore, the polar solvent molecules are on average symmetric around CV. At $S_{1,\mathrm{min}}$, due to two aniline rings being perpendicular to the third ring, CV has a dipole moment that points toward the third aniline ring.

Since the solvent is not arranged to favor a dipole in any specific direction, the newly formed dipole, when CV is excited, has an equal probability to be stabilized or destabilized by the solvent. Therefore, both k_{vis} and k_{IR} are close to zero initially. Then, in response to the newly formed dipole, the libration of the solvent molecules will stabilize CV and create a correlation between ω_{vis} and ω_{IR}. As a result, both k_{vis} and k_{IR} become non-zero and the magnitudes of both k_{vis} and k_{IR} increase during the first two picoseconds as solvent libration stabilizes the dipole. When CV goes through the conical intersection and arrives at the $S_{0,twist}$ geometry, the dipole moment flips 180° due to the change in the electronic structure. As a result, the stabilizing solvent environment becomes destabilizing, and both k_{vis} and k_{IR} switch sign. For MG, the CLSs are all the same sign, because the dipole moment does not change direction between $S_{0,eq}$, $S_{1,min}$, and $S_{0,twist}$. Therefore, the correlation between ω_{vis} and ω_{IR} is not affected during the entire relaxation process for MG.

One last comment on the signs of CLS, for CV in methanol, both k_{vis} and k_{IR} of the 1598 cm^{-1} peak become negative around waiting time of 2.5 ps. This is likely caused by the overlap between the 1598 cm^{-1} and 1589 cm^{-1} peaks.

Vibrational Peak Shapes and Intramolecular Charge Transfer

For both CV and MG, the 1577-cm^{-1} peak is initially broad and becomes sharper and blueshifts. Simulations by Terenziani *et al.* showed that the 2DEV spectrum for molecules with an ICT state has a broad excited state peak that sharpens and blueshifts as waiting time increases.[46] The initially broad excited peak is due to the nuclear wavepacket spreading out over the locally excited state and the intramolecular charge transfer state. Then as the wavepacket localizes into the ICT state, the excited peak sharpens. After photoexcitation, as the distribution of solvation coordinates evolve toward equilibrium and stabilize the charge transfer state, the mixing between the ground state and the ICT state becomes more effective. As the mixing between the two states increases, the excited state vibrational frequency increases. In addition to the calculations by Terenziani *et al.*, *ab initio* calculations show that CV and MG have ICT character in the excited state. The dominant virtual natural transition orbitals (NTOs)[47] at the $S_{1,FC}$ geometry (Figure 9 top left) is spread over the entire molecule, while the dominant virtual NTOs at the $S_{1,min}$ geometry (Figure 9 top right) is concentrated on one of the aniline groups. Therefore, as the rings twist and the nuclear wavepacket moves from the Franck-Condon region to the $S_{1,min}$, charge is transferred from two of the aniline rings onto the third one.

It is important to note that the intramolecular charge transfer revealed by the 2DEV spectra is different from the twisted intramolecular charge transfer (TICT) state reported by Nakayama *et al.*[31] In their experiment, the molecules relax to the TICT state after ~4 – 5 ps, and they assigned the stretch at 1589 cm^{-1} to the TICT state. Here, we found the excited state peak becomes sharp after ~1 – 2 ps, which is much shorter than the timescale reported by Nakayama, and we assigned the 1577 cm^{-1} peak to the ICT state. The relaxation from the FC region to the ICT state discussed here is likely what Xie *et al.* observed in their trajectories during the first 300 ps, where no population change was observed.

Symmetry of Crystal Violet

Finally, the symmetry of CV in solution has been debated in the past. Some authors argued that the symmetry of CV decreases from symmetric (D3) propeller to asymmetric (C2) propeller in which one of the phenyl rings is rotated counter to the other two when in solution.[48,49] However, more recently, others

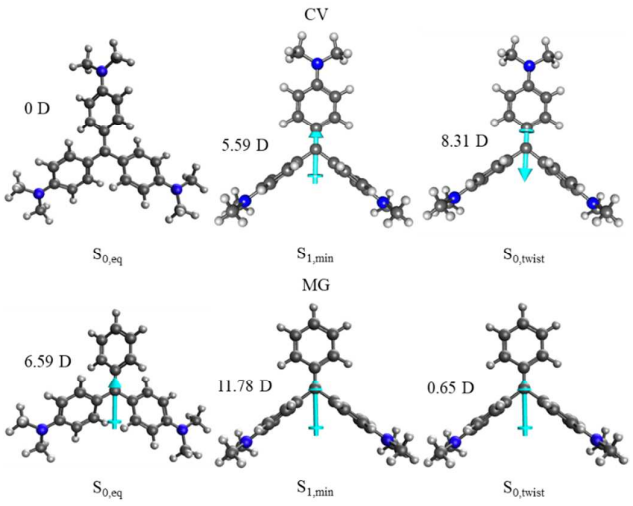

Figure 8. Calculated dipole moment of CV and MG at different optimized geometries, using TDDFT with the BHHLYP functional and 6-31G(d) basis set.

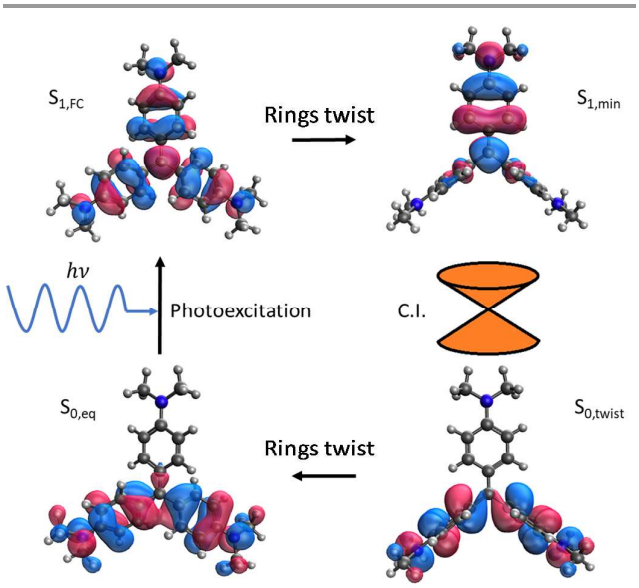

Figure 9. A cartoon illustrating the photoinduced excitation, subsequent evolution, and ultimate radiationless decay through a conical intersection of CV. The orbitals pictured are the dominant virtual NTOs for $S_{1,FC}$ and $S_{1,min}$ and the dominant occupied NTOs for $S_{0,eq}$, and $S_{0,twist}$.

argued that CV maintains the D3 symmetry in solution and the two overlapping bands observed in the absorption spectrum are caused by interactions with solvent that lift the degeneracy.[50–54] The 2DEV experiments performed do not seem to support
either hypothesis. If CV forms different complexes with the solvent or has different conformations, two sets of peaks should be observed, similar to those in the 2DEV spectra of chlorophyll b.[23,24] By comparing the pump spectra and the 2DEV spectra, the small peaks and other features observed around 1.8×10^4 cm^{-1} are likely due to the features of the pump laser, rather than molecular-based signals.

Conclusions

The 2DEV spectra of MG and CV in deuterated methanol and propanol showed that the relaxation of triphenylmethane dyes involves an intermediate and a conical intersection. Using the dynamics of peak intensities, we identified the intermediate as the twisted ground state, i.e. when the molecules have $S_{1,min}$ geometry on the ground state PES. We showed that the signs of the center line slopes can be explained by changes in the molecular dipole moment. With the support of electronic structure calculations, the broad excited state peaks in the 2DEV spectra can be interpreted to suggested that after photoexcitation, triphenylmethane dyes undergo intramolecular charge transfer. The combined experimental and theoretical results clearly show that interpreting the solvent dependence of triphenylmethane dye excited state lifetimes solely in terms of solvent viscosity as mechanical friction is inadequate. The large changes in charge distribution with dihedral angle mean that dielectric friction will also play an important role. It will be interesting to see if combined mechanical and dielectric friction models reproduce the well-known fractional dependence of fluorescence yield on solvent viscosity for a series of alcohol, for example.[29,55–61] In summary, this work demonstrates the advantages of applying 2DEV to study relaxation dynamics and to identify nuclear and electronic rearrangements, as well as their correlations. With the further development of theoretical models, 2DEV should prove to be a very useful probe of potential energy surfaces and the relaxation dynamics of complex molecules and complexes.

Conflicts of interest

There are no conflicts to declare.

Acknowledgements

Q.G. thanks Yuezhi Mao for helpful discussion. E.W., E.A.A., and G.R.F. were supported by NSF Grant CHE-1800345. Q.G. and M.H.G. were supported by the Director, Office of Science, Office of Basic Energy Sciences, of the U.S. Department of Energy under Contract No. DE-AC02-05CH11231. E.A.A. acknowledges the support of the Berkeley Fellowship.

Notes and references

1 M. A. Robb, 2014, vol. 48, pp. 189–228.
2 M. Garavelli, F. Bernardi, M. Olivucci, T. Vreven, S. Klein, P. Celani and M. a. Robb, *Faraday Discuss.*, 1998, **110**, 51–70.
3 H.-G. Duan and M. Thorwart, *J. Phys. Chem. Lett.*, 2016, **7**, 382–386.
4 M. H. Farag, T. L. C. Jansen and J. Knoester, *J. Phys. Chem. Lett.*, 2016, **7**, 3328–3334.
5 G. Herzberg and H. C. Longuet-Higgins, *Discuss. Faraday Soc.*, 1963, **35**, 77.
6 M. Garavelli, P. Celani, F. Bernardi, M. A. Robb and M. Olivucci, *J. Am. Chem. Soc.*, 1997, **119**, 11487–11494.
7 D. R. Yarkony, *Rev. Mod. Phys.*, 1996, **68**, 985–1013.
8 W. Domcke, D. Yarkony and H. Koppel, *Conical Intersections - Electronic Structure, Dynamics and Spectroscopy*, World Scientific Publishing Co. Pte. Ltd., 2004, vol. 15.
9 T. A. A. Oliver and G. R. Fleming, *J. Phys. Chem. B*, 2015, **119**, 11428–11441.
10 T. A. A. Oliver, N. H. C. Lewis and G. R. Fleming, *Following the Excited State Dynamics of β-apo-8'-carotenal with Two-Dimensional Electronic-Vibrational Spectroscopy*, Springer International Publishing, Cham, 2015, vol. 162.
11 M. Liebel, C. Schnedermann and P. Kukura, *Phys. Rev. Lett.*, 2014, **112**, 198302.
12 H. Satzger, D. Townsend, M. Z. Zgierski, S. Patchkovskii, S. Ullrich and A. Stolow, *Proc. Natl. Acad. Sci. U. S. A.*, 2006, **103**, 10196–10201.
13 H. R. Hudock, B. G. Levine, A. L. Thompson, H. Satzger, D. Townsend, N. Gador, S. Ullrich, A. Stolow and T. J. Martínez, *J. Phys. Chem. A*, 2007, **111**, 8500–8508.
14 G. Groenhof, L. V. Schäfer, M. Boggio-Pasqua, M. Goette, H. Grubmüller and M. A. Robb, *J. Am. Chem. Soc.*, 2007, **129**, 6812–6819.
15 H. R. Hudock and T. J. Martínez, *ChemPhysChem*, 2008, **9**, 2486–2490.
16 Z. Wei, T. Nakamura, S. Takeuchi and T. Tahara, *J. Am. Chem. Soc.*, 2011, **133**, 8205–8210.
17 D. Polli, P. Altoè, O. Weingart, K. M. Spillane, C. Manzoni, D. Brida, G. Tomasello, G. Orlandi, P. Kukura, R. A. Mathies, M. Garavelli and G. Cerullo, *Nature*, 2010, **467**, 440–443.
18 V. I. Prokhorenko, *Science (80-.).*, 2006, **313**, 1257–1261.
19 D. P. Hoffman, S. R. Ellis and R. A. Mathies, *J. Phys. Chem. A*, 2014, **118**, 4955–4965.
20 N. H. C. Lewis, H. Dong, T. A. A. Oliver and G. R. Fleming, *J. Chem. Phys.*, 2015, **142**, 174202.
21 T. A. A. Oliver, N. H. C. Lewis and G. R. Fleming, *Proc. Natl. Acad. Sci.*, 2014, **111**, 10061–10066.
22 H. Dong, N. H. C. Lewis, T. A. A. Oliver and G. R. Fleming, *J. Chem. Phys.*, 2015, **142**, 174201.
23 N. H. C. Lewis and G. R. Fleming, *J. Phys. Chem. Lett.*, 2016, **7**, 831–837.
24 N. H. C. Lewis, N. L. Gruenke, T. A. A. Oliver, M. Ballottari, R. Bassi and G. R. Fleming, *J. Phys. Chem. Lett.*, 2016, **7**, 4197–4206.
25 A. J. Lewis, A. Ruseckas, O. P. M. Gaudin, G. R. Webster, P.

L. Burn and I. D. W. Samuel, *Org. Electron.*, 2006, **7**, 452–456.
26 A. C. Bhasikuttan, A. V Sapre and T. Okada, *J. Phys. Chem. A*, 2003, **107**, 3030–3035.
27 S. Rafiq, R. Yadav and P. Sen, *J. Phys. Chem. B*, 2010, **114**, 13988–13994.
28 M. Yoshizawa, K. Suzuki, A. Kubo and S. Saikan, *Chem. Phys. Lett.*, 1998, **290**, 43–48.
29 M. D. Hirsch and H. Mahr, *Chem. Phys. Lett.*, 1979, **60**, 299–303.
30 B. Bagchi, G. R. Fleming and D. W. Oxtoby, *J. Chem. Phys.*, 1983, **78**, 7375–7385.
31 A. Nakayama and T. Taketsugu, *J. Phys. Chem. A*, 2011, **115**, 8808–8815.
32 B.-B. Xie, S.-H. Xia, L.-H. Liu and G. Cui, *J. Phys. Chem. A*, 2015, **119**, 5607–5617.
33 G. Li, D. Magana and R. B. Dyer, *J. Phys. Chem. B*, 2012, **116**, 12590–12596.
34 J. A. Myers, K. L. Lewis, P. F. Tekavec and J. P. Ogilvie, *Opt. Express*, 2008, **16**, 17420.
35 J. A. Myers, *Methods*.
36 Y. Shao, M. Head-Gordon and A. I. Krylov, *J. Chem. Phys.*, 2003, **118**, 4807–4818.
37 S. Hirata and M. Head-Gordon, *Chem. Phys. Lett.*, 1999, **314**, 291–299.
38 A. Dreuw and M. Head-Gordon, *Chem. Rev.*, 2005, **105**, 4009–4037.
39 M. A. L. Marques and E. K. U. Gross, *Annu. Rev. Phys. Chem.*, 2004, **55**, 427–455.
40 S. J. A. van Gisbergen, J. G. Snijders and E. J. Baerends, *Comput. Phys. Commun.*, 1999, **118**, 119–138.
41 M. E. Casida, *J. Mol. Struct. THEOCHEM*, 2009, **914**, 3–18.
42 T. Ziegler, A. Rauk and E. J. Baerends, *Theor. Chim. Acta*, 1977, **43**, 261–271.
43 A. D. Becke, *J. Chem. Phys.*, 1993, **98**, 1372–1377.
44 P. C. Hariharan and J. A. Pople, *Theor. Chim. Acta*, 1973, **28**, 213–222.
45 Y. Shao, Z. Gan, E. Epifanovsky, A. T. B. Gilbert, M. Wormit, J. Kussmann, A. W. Lange, A. Behn, J. Deng, X. Feng, D. Ghosh, M. Goldey, P. R. Horn, L. D. Jacobson, I. Kaliman, R. Z. Khaliullin, T. Kuś, A. Landau, J. Liu, E. I. Proynov, Y. M. Rhee, R. M. Richard, M. A. Rohrdanz, R. P. Steele, E. J. Sundstrom, H. L. Woodcock, P. M. Zimmerman, D. Zuev, B. Albrecht, E. Alguire, B. Austin, G. J. O. Beran, Y. A. Bernard, E. Berquist, K. Brandhorst, K. B. Bravaya, S. T. Brown, D. Casanova, C.-M. Chang, Y. Chen, S. H. Chien, K. D. Closser, D. L. Crittenden, M. Diedenhofen, R. A. DiStasio, H. Do, A. D. Dutoi, R. G. Edgar, S. Fatehi, L. Fusti-Molnar, A. Ghysels, A. Golubeva-Zadorozhnaya, J. Gomes, M. W. D. Hanson-Heine, P. H. P. Harbach, A. W. Hauser, E. G. Hohenstein, Z. C. Holden, T.-C. Jagau, H. Ji, B. Kaduk, K. Khistyaev, J. Kim, J. Kim, R. A. King, P. Klunzinger, D. Kosenkov, T. Kowalczyk, C. M. Krauter, K. U. Lao, A. D. Laurent, K. V. Lawler, S. V. Levchenko, C. Y. Lin, F. Liu, E. Livshits, R. C. Lochan, A. Luenser, P. Manohar, S. F. Manzer, S.-P. Mao, N. Mardirossian, A. V. Marenich, S. A. Maurer, N. J. Mayhall, E. Neuscamman, C. M. Oana, R. Olivares-Amaya, D. P. O'Neill, J. A. Parkhill, T. M. Perrine, R. Peverati, A. Prociuk, D. R. Rehn, E. Rosta, N. J. Russ, S. M. Sharada, S. Sharma, D. W. Small, A. Sodt, T. Stein, D. Stück, Y.-C. Su, A. J. W. Thom, T. Tsuchimochi, V. Vanovschi, L. Vogt, O. Vydrov, T. Wang, M. A. Watson, J. Wenzel, A. White, C. F. Williams, J. Yang, S. Yeganeh, S. R. Yost, Z.-Q. You, I. Y. Zhang, X. Zhang, Y. Zhao, B. R. Brooks, G. K. L. Chan, D. M. Chipman, C. J. Cramer, W. A. Goddard, M. S. Gordon, W. J. Hehre, A. Klamt, H. F. Schaefer, M. W. Schmidt, C. D. Sherrill, D. G. Truhlar, A. Warshel, X. Xu, A. Aspuru-Guzik, R. Baer, A. T. Bell, N. A. Besley, J.-D. Chai, A. Dreuw, B. D. Dunietz, T. R. Furlani, S. R. Gwaltney, C.-P. Hsu, Y. Jung, J. Kong, D. S. Lambrecht, W. Liang, C. Ochsenfeld, V. A. Rassolov, L. V. Slipchenko, J. E. Subotnik, T. Van Voorhis, J. M. Herbert, A. I. Krylov, P. M. W. Gill and M. Head-Gordon, *Mol. Phys.*, 2015, **113**, 184–215.
46 F. Terenziani and A. Painelli, *Phys. Chem. Chem. Phys.*, 2015, **17**, 13074–13081.
47 R. L. Martin, *J. Chem. Phys.*, 2003, **118**, 4775–4777.
48 H. P. J. M. Dekkers and M. E. C. M. Kielman-Van Luyt, *Mol. Phys.*, 1976, **31**, 1001–1019.
49 G. N. Lewis, T. T. Magel and D. Lipkin, *J. Am. Chem. Soc.*, 1942, **64**, 1774–1782.
50 H. B. Lueck, J. L. McHale and W. D. Edwards, *J. Am. Chem. Soc.*, 1992, **114**, 2342–2348.
51 J. Korppi-Tommola and R. W. Yip, *Can. J. Chem.*, 1981, **59**, 191–194.
52 J. Korppi-Tommola, E. Kolehmainen, E. Salo and R. W. Yip, *Chem. Phys. Lett.*, 1984, **104**, 373–377.
53 L. Angeloni, G. Smulevich and M. P. Marzocchi, *J. Raman Spectrosc.*, 1979, **8**, 305–310.
54 S. Sunder and H. J. Bernstein, *Can. J. Chem.*, 1981, **59**, 964–967.
55 T. Förster and G. Hoffmann, *Zeitschrift für Phys. Chemie*, 1971, **75**, 63–76.
56 L. A. Brey, G. B. Schuster and H. G. Drickamer, *J. Chem. Phys.*, 1977, **67**, 2648.
57 P. Wirth, S. Schneider and F. Dörr, *Opt. Commun.*, 1977, **20**, 155–158.
58 W. Yu, F. Pellegrino, M. Grant and R. R. Alfano, *J. Chem. Phys.*, 1977, **67**, 1766–1773.
59 C. J. Mastrangelo and H. W. Offen, *Chem. Phys. Lett.*, 1977, **46**, 588–590.
60 D. Magde and M. W. Windsor, *Chem. Phys. Lett.*, 1974, **24**, 144–148.
61 E. P. Ippen, C. V. Shank and A. Bergman, *Chem. Phys. Lett.*, 1976, **38**, 611–614.